Spatial resolution correction for wall-bounded turbulence measurements

A. J. SMITS, J. MONTY, M. HULTMARK, S. C. C. BAILEY, N. HUTCHINS and I. MARUSIC

Journal of Fluid Mechanics / Volume 676 / June 2011, pp 41 - 53
DOI: 10.1017/jfm.2011.19, Published online: 06 April 2011

J. Fluid Mech. (2011), *vol.* 676, *pp.* 41–53.
doi:10.1017/jfm.2011.19

Spatial resolution correction for wall-bounded turbulence measurements

A. J. SMITS[1]†, J. MONTY[2], M. HULTMARK[1], S. C. C. BAILEY[3], N. HUTCHINS[2] AND I. MARUSIC[2]

[1]Department of Mechanical and Aerospace Engineering, Princeton University, Princeton, NJ 08544, USA

[2]Department of Mechanical Engineering, University of Melbourne, Victoria 3010, Australia

[3]Department of Mechanical Engineering, University of Kentucky, Lexington, KY 40506, USA

(Received 17 September 2010; revised 4 December 2010; accepted 4 January 2011; first published online 6 April 2011)

A correction for streamwise Reynolds stress data acquired with insufficient spatial resolution is proposed for wall-bounded flows. The method is based on the attached eddy hypothesis to account for spatial filtering effects at all wall-normal positions. This analysis reveals that outside the near-wall region the spatial filtering effect scales inversely with the distance from the wall, in contrast to the commonly assumed scaling with the viscous length scale. The new formulation is shown to work very well for data taken over a wide range of Reynolds numbers and wire lengths.

Key words: shear layer turbulence, turbulent boundary layers, turbulent flows

1. Introduction

In recent years there has been a heightened interest in the behaviour of high Reynolds number, wall-bounded turbulent flows, which are important to large-scale applications, including atmospheric flows (Marusic *et al.* 2010). Accordingly, a number of new facilities that provide detailed access to high Reynolds number flows have been commissioned, including the Princeton/ONR Superpipe (Zagarola & Smits 1998) and High Reynolds Number Test Facility (Jiménez, Hultmark & Smits 2010), the Stanford pressurized wind tunnel (DeGraaff & Eaton 2000), the MTL wind tunnel at KTH (Österlund *et al.* 2000), the National Diagnostic Facility at IIT (Nagib, Chauhan & Monkewitz 2007) and the High Reynolds Number Boundary Layer Wind Tunnel at the University of Melbourne (Nickels *et al.* 2007). In addition, the Surface Layer Turbulence and Environmental Science Test (SLTEST) facility in Utah (Metzger & Klewicki 2001) has provided high quality data in the atmospheric boundary layer, which has been invaluable for studying the behaviour at Reynolds numbers one or two orders of magnitude larger than what is possible in the laboratory. Other, more general purpose facilities, have also been employed to study high Reynolds number boundary layer flows, including the NASA Ames Full-Scale Aerodynamics Facility (Saddoughi & Veeravalli 1994), DNW, the German–Dutch wind tunnel (Fernholz *et al.* 1995) and the US Navy's William B. Morgan Large Cavitation Channel (Etter *et al.* 2005; Winkel *et al.* 2010).

† Email address for correspondence: asmits@princeton.edu

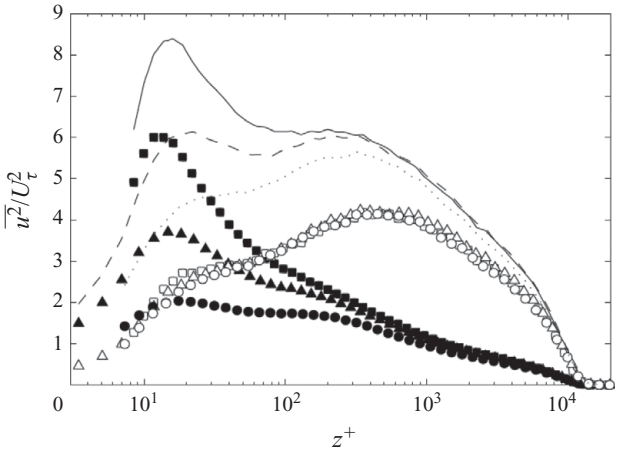

FIGURE 1. Streamwise Reynolds stress profiles decomposed into small-scale ($\lambda_x < \delta$, solid symbols) and large-scale components ($\lambda_x > \delta$, open symbols), where □, $l^+ = 22$; △, $l^+ = 79$; and ○, $l^+ = 153$. The lines show sum of small- and large-scale components for $l^+ = 22$ (solid line), $l^+ = 79$ (dashed line) and $l^+ = 153$ (dotted line). Here, $Re_\tau = 13\,600$. Taken from Hutchins *et al.* (2009).

One of the main questions that has arisen from these studies is the scaling of the streamwise Reynolds stress $\overline{u^2}$, particularly the behaviour of the near-wall peak found at about $z^+ = 15$. Here, $z^+ = zu_\tau/\nu$, $u_\tau = \sqrt{(\tau_w/\rho)}$, τ_w is the wall shear stress, z is the wall-normal distance, and ρ and ν are the fluid density and kinematic viscosity, respectively. Wall-scaling arguments based on the behaviour of the mean velocity profile suggest that $\overline{u^2}^+ = \overline{u^2}/u_\tau^2$ should be invariant with z^+ in the near-wall region, as supported by the pipe flow studies by Mochizuki & Nieuwstadt (1996) and Hultmark, Bailey & Smits (2010). However, boundary layer investigations by, for example, DeGraaff & Eaton (2000) and Metzger & Klewicki (2001) show a clear increase in the peak value with increasing Reynolds number. Another issue that has arisen is that of the appearance of a second peak in the $\overline{u^2}^+$ profile at high Reynolds number. For example, Morrison *et al.* (2004) found that in a pipe, at sufficiently high Reynolds numbers an outer peak was formed, located near the lower edge of the log-region. This behaviour was also seen in the boundary layer measurements taken in the DNW by Fernholz *et al.* (1995).

One of the principal reasons why these scaling issues remain unresolved is that the spatial resolution of hot wire probes is often insufficient to make accurate turbulence measurements near the wall, where the smallest scales of turbulence are found. Because the size of the smallest scales decreases with increasing Reynolds number, the effects of spatial filtering become more important at high Reynolds number, and they can potentially obscure the true Reynolds number behaviour. For example, spatial resolution can mask the growth of the inner peak, and it can artificially create the appearance of an outer peak in the profile because of spurious filtering of the near-wall energy.

Such spatial resolution effects are illustrated in figure 1. Here, three different sized hot-wires with $l^+ = lu_\tau/\nu = 22$, 79 and 153 were used to measure the same wall-normal profile of streamwise Reynolds stress, at a single Reynolds number $Re_\tau = \delta u_\tau/\nu = 13\,600$, where δ is the boundary layer thickness and l is the wire length. Strong attenuation is noted for the larger sensing elements, and it is clear how spatial

filtering could artificially create the outer peak. Also shown in figure 1 is what happens when the velocity signal is partitioned into large and small length scale contributions by applying a sharp spectral filter with a cutoff length λ_x equal to the boundary layer thickness. As expected, the attenuation observed for the larger values of l^+ are mostly confined to under-resolving the small-scale contributions to the broadband intensity.

Although the values of l^+ used to obtain these results may seem large, they are not atypical of high Reynolds number experiments. For example, in the Princeton Superpipe at $Re_\tau = 10^5$, $l^+ = 100$ corresponds to a wire length of $l = 65$ μm, and the smallest wires used in conventional hot-wire anemometry are typically larger than about 250 μm. For this reason, considerable effort is currently being devoted to the design and development of new sub-miniature hot-wires using micro- and nano-fabrication techniques such as the Nano Scale Thermal Anemometry Probe (NSTAP) developed at Princeton (Bailey *et al.* 2010).

Notwithstanding these micro-probe advances, there is a continuing need to better understand and quantify the effects of spatial resolution, particularly in the near-wall region. A widely used analysis of spatial resolution is that proposed by Wyngaard (1968), and it is based, as many other methods are, on the assumption of small-scale isotropy. In the near-wall region, however, the flow is strongly anisotropic. The analysis by Cameron *et al.* (2010), based on a two-dimensional spectral representation, demonstrates the significant role of anisotropy in the spatial filtering behaviour of a hot wire, and also shows how the filtering can significantly affect the energy spectrum at wavenumbers much smaller than that corresponding to the wire length. Recently, Chin *et al.* (2009) proposed a correction method where a detailed account of the missing energy is modelled using the spanwise-streamwise information in two-dimensional spectra from a direct numerical simulation (DNS) of turbulent channel flow. The approach appears to be promising, despite being rather complicated. Monkewitz, Duncan & Nagib (2010) have suggested an empirical correction method that also shows potential.

Here, we propose a new correction method for spatial filtering based on eddy scaling. The method corrects for the effects of spatial resolution across the entire boundary layer, and it appears to give accurate results over a very wide range of wire lengths and flow Reynolds numbers. The success of the method appears to be due mostly to the fact that, outside the near-wall viscous region, it uses the correct length scale, which is the distance from the wall rather than the viscous length scale adopted by most previous authors (see, for example, Ligrani & Bradshaw 1987; Monkewitz *et al.* 2010).

2. Near-wall eddy scales

The results shown in figure 1 suggest that modelling the effects of spatial filtering requires knowledge of the local small-scale eddies that contribute to the turbulence intensities. Here we consider that connection more closely.

We begin with the observation by Hutchins *et al.* (2009), who used a series of wires with $11 < l^+ < 153$ over a range of Reynolds number to determine that the missing energy at $y^+ = 15$ can be described by a relationship that is linear in l^+. That is,

$$\Delta\overline{u^2}^+ = B_1 l^+ + C_1 \left(\frac{l^+}{Re_\tau} \right), \tag{2.1}$$

where $B_1 = 0.0352$ and $C_1 = 23.0833$. However, we would expect that when l^+ is very small the results should be independent of wire length since the smallest eddies are

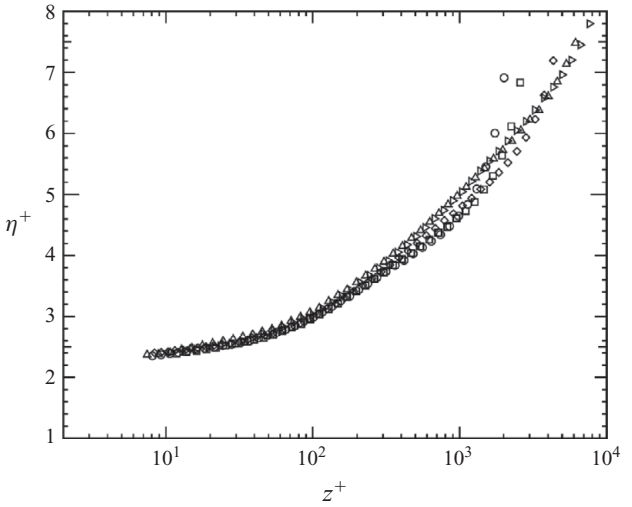

FIGURE 2. Kolmogorov length scale with wall scaling across turbulent boundary layers. Data as in Hutchins *et al.* (2009). Here, $\eta = (\nu^3/\epsilon)^{1/4}$, where the isotropic assumption is used to estimate the dissipation rate: $\epsilon = 15\nu \int_0^\infty k_x^2 \phi_{uu}\, \mathrm{d}k_x$. Symbols indicated Re_τ values: ○ 2800, □ 3900, ◇ 7300, △ 13 600, ▷ 19 000.

fully resolved. Hence the behaviour for small l^+ might be very different from that of large l^+. Chin *et al.* (2009) used filtered DNS data to find a correlation that captures this variation more accurately, and proposed instead a third-order function in l^+, with no dependence on Re_τ. That is,

$$\Delta\overline{u^2}^+ = A_2 l^{+3} + B_2 l^{+2} + C_2 l^+ + D_2, \tag{2.2}$$

with $A_2 = -1.94 \times 10^{-5}$, $B_2 = 1.83 \times 10^{-3}$, $C_2 = 1.76 \times 10^{-2}$ and $D_2 = -9.68 \times 10^{-2}$. Note that this polynomial relationship is not well behaved at large values of l^+ so that it can only be used up to $l^+ \approx 30$.

Hutchins *et al.* (2009) and Chin *et al.* (2009) assume that l^+ is the appropriate scaling for spatial filtering effects, which is in accordance with much of the previous work, including the influential study by Ligrani & Bradshaw (1987). This viscous scaling is consistent with the findings of Kline *et al.* (1967) and many others that the near-wall streaks scale with wall units over a large Reynolds number range, with a spacing of nominally $100\nu/u_\tau$. Furthermore, there is strong evidence to suggest that the near-wall streaks are a manifestation, or at least are associated with, the legs of near-wall attached eddies as described by Perry & Chong (1982) and Adrian (2007), where the size of the smallest attached eddies is $O(100\nu/u_\tau)$.

Nonetheless, the smallest motions in any turbulent flow scale with the Kolmogorov length scale η, and consequently the effects of spatial resolution should also depend on l/η and not simply l^+. For example, recent studies by Stanislas, Perret & Foucaut (2008) and others have shown that in boundary layers the core diameter of the smallest filamentary vortex structures (and likely the segments of the energy-containing eddies) are $O(12\eta)$. However, we see from figure 2 that in the near-wall region (say, $z^+ < 50$) η^+ is almost constant, so that η and ν/u_τ are not independent. Note also that, across the entire inner-region including the log region, η^+ is virtually invariant with the Reynolds number. Similar results were also found by Carlier & Stanislas (2005) and

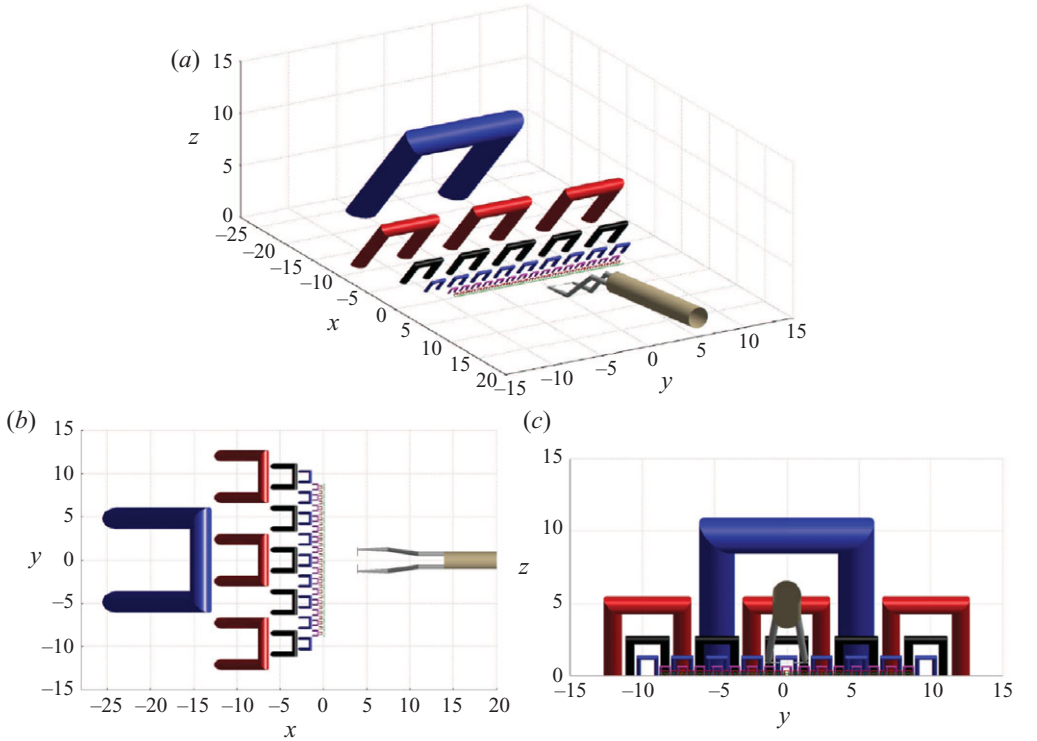

FIGURE 3. (Colour online) (*a*) Scale drawing of a hot-wire sensing an artificially arrayed sample of idealized attached eddies. It may be seen that the wire will resolve fewer eddies as the wall is approached. Top (*b*) and front (*c*) views are also shown. The flow is in the x-direction and distances are in arbitrary units.

Yakhot, Bailey & Smits (2010) across a large range of Reynolds number in pipe flows.

What about the outer region where η^+ varies with wall distance? Given that far from the wall the eddy core sizes continue to scale with η (Stanislas *et al.* 2008), this implies that the Kolmogorov length should remain a relevant scale for the unresolved energy so long as $\eta < l$. When such eddies inevitably 'die', their filaments are effectively broken up leading to motions scaling exclusively with η. Therefore, there will be some measure of unresolved energy even at large wall-distances which should scale as l/η.

Since the greatest filtering effects occur close to the wall where $\eta u_\tau/\nu$ is approximately constant, it therefore should not matter whether we choose l^+ or l/η for scaling the effect of wire length. In order to be consistent with the traditional approach (that is, as used by Hutchins *et al.* 2009) we will express our scaling in terms of l^+, even though l/η may be more physically appropriate. In addition, l^+ is a more practical parameter because for unresolved measurements the behaviour of η is not known accurately.

If we now consider the region outside the viscous wall region, then according to Townsend's (1976) attached eddy hypothesis, the energy-containing scales of turbulence scale with distance from the wall. Figure 3 illustrates this concept using idealized hairpin shaped eddies as originally proposed by Perry & Chong (1982). In their model, wall-bounded turbulence may be described by hierarchies of attached eddies, the smallest being of $O(100\nu/u_\tau)$ and thereafter following a geometric

progression in size, with the largest being approximately the height of the boundary layer. Therefore, these eddies can be taken as the major contributors to the small-scale energy, which we are interested in modelling for purposes of estimating the effects of spatial filtering.

The concept of eddy hierarchies is illustrated in figure 3 by schematically lining up eddies of each scale. The distribution of hierarchies is such that there are many more small eddies than large eddies, and Townsend (1976) proposed that the probability density function of eddy sizes should be inversely proportional to the eddy size in order to give a region of constant Reynolds shear stress. In figure 3, a typical hot-wire probe is shown, having a sensor width approximately the same size as the fourth largest hierarchy of eddies illustrated in this drawing. At the wall-normal distance of the probe shown in the figure, the sensor would capture most of the contributions from the eddies of this size and above. However, as the sensor moves down, it is clear that it will begin to filter contributions from the smaller eddies at an increasing rate. It can be shown that the attenuation in energy is a function of l/z if an inverse probability density function of eddy sizes is chosen. If we assume a cutoff factor γ exists such that eddies smaller than γl are not resolved at all and eddies larger than γl are fully resolved, then

$$(\overline{u^2}^+)_{unresolved} = C_1 \log\left(\frac{\gamma l}{z}\right). \tag{2.3}$$

Hence the attached eddy hypothesis suggests that the attenuation due to finite fixed sensor size should be a function of l/z, simply because eddy size increases rapidly with wall-distance.

It should be noted that the attached eddy argument leading to the logarithmic dependence is a result that only holds true in the asymptotic limit of very high Reynolds number. For finite Reynolds number, Marusic & Kunkel (2003) have shown that the logarithmic scaling of the turbulence intensity is limited to a small region of the flow and viscous and eddy cutoff corrections are required to reproduce these statistics. This highlights that there are other important contributions to spatial filtering that should be accounted for in addition to these idealized attached eddies, but accounting for such contributions is a difficult task and is beyond the scope of this paper. However, the attached eddy model suggests a scaling with l/z, which will become important as we shall see.

3. Formulation for the unresolved energy

By using the attached eddy scaling argument, we can extend the conclusions made by Hutchins *et al.* (2009) and Chin *et al.* (2009) regarding the filtered energy $\Delta\overline{u^2}$ at the location of the inner peak to all wall-normal positions.

The analysis of Wyngaard (1968) and others for isotropic turbulence indicate that the spatial filtering affects the measured spectra F according to:

$$F(\kappa_1 l) = \int_{-\infty}^{\infty}\int_{-\infty}^{\infty} \Phi_{11}(\kappa) H(\kappa_2, l)\,\mathrm{d}\kappa_2\,\mathrm{d}\kappa_3, \tag{3.1}$$

where κ_1, κ_2 and κ_3 are, respectively, the wavenumbers in the direction of the flow, in the direction along the wire and in the direction mutually perpendicular to the wire and the flow. Also, Φ_{11} is the streamwise normal component of the true spectral density tensor and H is a filter function representing the attenuation of energy as a function of wire length and wire-direction wavenumber.

Therefore, it seems more appropriate to approach the problem of spatial filtering using a multiplicative factor between the true and measured values, rather than examining the difference between them, which is the approach used in Hutchins *et al.* (2009) and Chin *et al.* (2009). Starting with this observation, we can propose that the attenuation of the streamwise Reynolds stress due to spatial filtering takes the form

$$\overline{u^2}^+_m = g_1(l^+, z^+)\overline{u^2}^+_T, \tag{3.2}$$

or

$$\frac{\Delta\overline{u^2}^+}{\overline{u^2}^+_m} = \frac{1}{g_1(l^+, z^+)} - 1 = g_2(l^+, z^+), \tag{3.3}$$

where $\overline{u^2}_T$ and $\overline{u^2}_m$ are the true and measured streamwise Reynolds stress respectively, and $\Delta\overline{u^2} = \overline{u^2}_T - \overline{u^2}_m$.

For a measurement at a single Reynolds number and a fixed wire length, l^+ will be constant so that we can propose a form for g_2 as follows:

$$\frac{\Delta\overline{u^2}^+}{\overline{u^2}^+_m} = M(l^+)f(z^+). \tag{3.4}$$

Because M is a constant for all z^+ locations, it only needs to be found at one location. We can find a first approximation to M by using the result for $\Delta\overline{u^2}^+$ at the near-wall peak obtained by Hutchins *et al.* (2009, (2.1)) and letting $f(z^+) = 1$ at $z^+ = 15$ such that

$$M = \frac{B_1(l^+) + C_1(l^+/Re_\tau)}{\overline{u^2}^+_m|_{z^+=15}}. \tag{3.5}$$

However, it was noted by Chin *et al.* (2009) that the form given by Hutchins *et al.* (2009) has a non-physical behaviour for $l^+ \lesssim 10$ and over-corrects the peak for $l^+ \gtrsim 100$, since nonlinearities become important for larger wire lengths. Using the correlation suggested by Chin *et al.* (2009) for $l^+ < 23$ (which is based on DNS data) along with experimental data from Hutchins *et al.* (2009) and Ng *et al.* (2011), we find that

$$\Delta\overline{u^2}^+|_{z^+=15} = A\tanh(\alpha l^+)\tanh(\beta l^+ - E), \tag{3.6}$$

where $A = 6.13$, $\alpha = 5.6 \times 10^{-2}$, $\beta = 8.6 \times 10^{-3}$ and $E = -1.26 \times 10^{-2}$ (these are fitting parameters with no particular physical meaning). Equation (3.6) applies over a broader range of l^+ than either (2.1) or (2.2). Note that in (3.6) we have neglected the l^+/Re_τ term under the assumption that l/δ will be negligibly small for most cases where a correction is applied. Also, because the true values of $\Delta\overline{u^2}^+$ are unknown for the experimental data, they were estimated using the data for $l^+ = 22$ and adjusted using the correlation by Chin *et al.* (2009) according to:

$$\Delta\overline{u^2}^+ = \overline{u^2}^+_m|_{l^+=22} - \overline{u^2}^+_m + \Delta\overline{u^2}^+_{Chin}(l^+ = 22). \tag{3.7}$$

Figure 4 illustrates the accuracy of this new correlation over the range $0 < l^+ < 150$.

Equation (3.6) can now be used in (3.4) to find M at $z^+ = 15$:

$$M = \left.\frac{\Delta\overline{u^2}^+}{\overline{u^2}^+_m}\right|_{z^+=15} = \frac{A\tanh(\alpha l^+)\tanh(\beta l^+ - E)}{(\overline{u^2}^+_m)_{z^+=15}}, \tag{3.8}$$

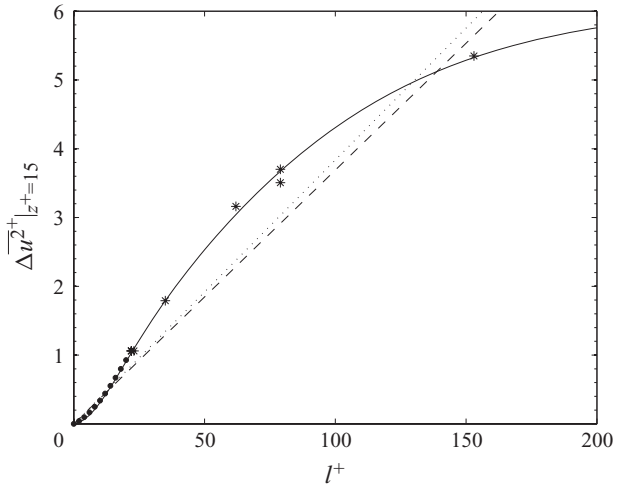

FIGURE 4. The missing energy, at $z^+ = 15$, as a function of wire length in wall units. Solid line is (3.6); • is the correlation given in Chin *et al.* (2009), and ∗ experimental data from Hutchins *et al.* (2009) and Ng *et al.* (2011). The dashed line and the dotted line are the linear correlations given by Hutchins *et al.* (2009) at $Re_\tau = 13\,600$ and $Re_\tau = 7300$, respectively.

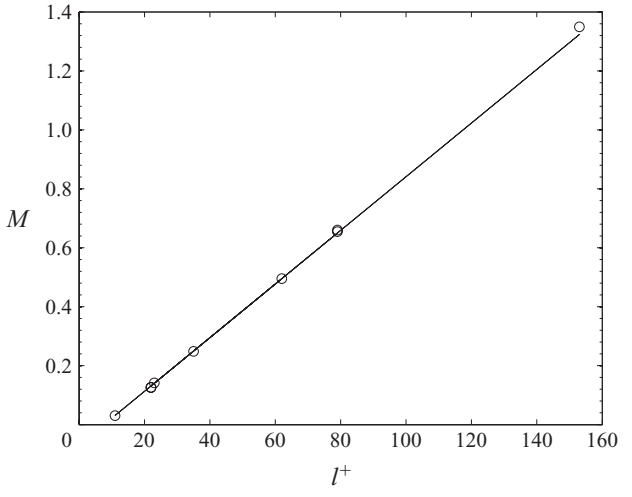

FIGURE 5. $M(l^+)$ from the experimental data with the linear fit given by (3.9), to be used if no direct measurements of $\overline{u^2}$ are available at $z^+ = 15$.

and so the function M is now known if a direct measurement of $\overline{u^2}_m$ is available at $z^+ = 15$.

When the data from figure 4 are used to calculate M, as is done in figure 5, the resulting function appears to be almost perfectly linear, which is entirely in accord with the attached eddy argument that suggested that the attenuation should scale with l/z. Note that in many cases, especially at high Reynolds number, $(\overline{u^2}_m)_{z^+=15}$ can be difficult to obtain. In that case, one can instead use the regression fit

$$M = 0.0091l^+ - 0.069, \tag{3.9}$$

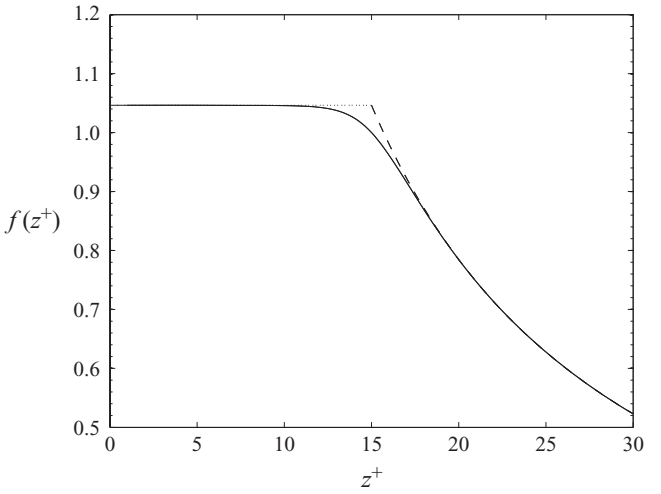

FIGURE 6. The behaviour of $f(z^+)$, dotted line the low z^+ asymptote and dashed line the high z^+. Solid line is the functional form as given in (3.11).

which is shown in figure 5 together with the experimental data. A note of caution is warranted here, in that (3.9) should only be used when no measurement of the peak is available. Also, (3.9) implies that a sensor length of $l^+ \leqslant 8$ will fully resolve the flow, whereas in practice it seems that we need $l^+ \leqslant 4$.

We can now seek the form of $f(z^+)$. Based on the attached eddy hypothesis, we propose that the function $f(z^+)$ will have three defining characteristics. Firstly, in the viscous region, the Kolmogorov scale is the relevant scale, and since η^+ is nearly constant for $z^+ < 15$, we expect the attenuation to be also constant in this region, given by $f = k_1$, where k_1 is a constant close to unity. Secondly, f must be unity at $z^+ = 15$. Thirdly, in § 2 it was argued that an l/z dependence is likely, therefore f is expected to vary as k_2/z for $z^+ > 15$, where k_2 is a constant.

In summary,

$$f(z^+) = \begin{cases} k_1 & z^+ \ll 15, \\ 1 & z^+ = 15, \\ k_2/z^+ & z^+ \gg 15. \end{cases} \tag{3.10}$$

In order to avoid discontinuities and to present a single functional form for $f(z^+)$ that obeys these limits, (3.10) can be represented using a modified rounded ramp function (Lagerlof 1974). That is

$$f(z^+) = \frac{15 + \ln(2)}{z^+ + \ln\left[\mathrm{e}^{(15-z^+)} + 1\right]} \tag{3.11}$$

which is compared to (3.10) in figure 6.

Everything is now in place to correct the streamwise Reynolds stress measured using a finite length sensor to the value it would have if it had been acquired with an infinitesimally small sensor ($l^+ = 0$). That is,

$$\overline{u^2}^+_T = \left[M(l^+) f(z^+) + 1\right] \overline{u^2}^+_m. \tag{3.12}$$

The correction proposed here should apply equally well to boundary layers, pipe flows and channel flows.

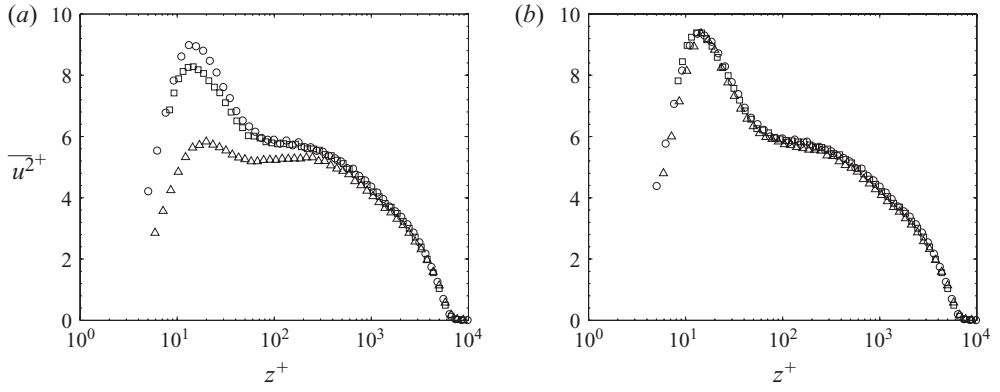

FIGURE 7. Streamwise Reynolds stress profiles measured in a turbulent boundary layer with various wire lengths at $Re_\tau = 7300$, where $\circ\ l^+ = 11$, $\square\ l^+ = 23$ and $\triangle\ l^+ = 79$: (*a*) uncorrected data, (*b*) streamwise Reynolds stress profiles corrected using the proposed correction, using the measured value of $\overline{u^2}^+_m$ at $z^+ = 15$. Data from Hutchins *et al.* (2009).

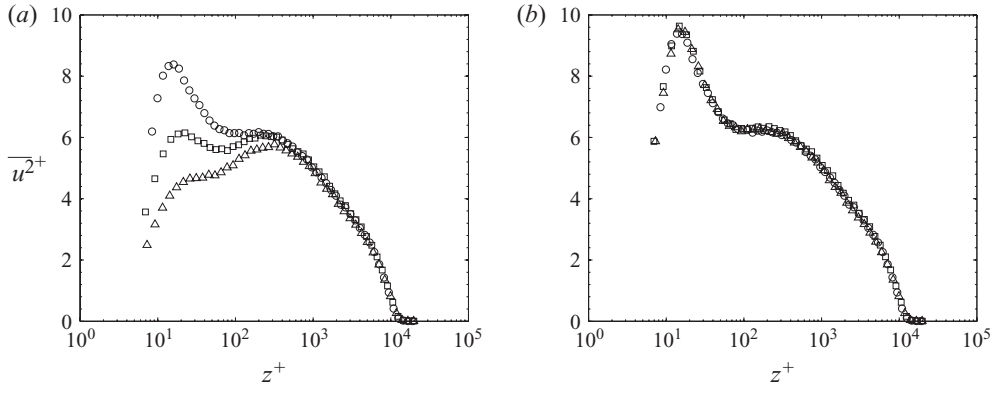

FIGURE 8. Streamwise Reynolds stress profiles measured in a turbulent boundary layer with various wire lengths at $Re_\tau = 13\,600$, where $\circ\ l^+ = 22$, $\square\ l^+ = 79$ and $\triangle\ l^+ = 153$: (*a*) uncorrected data, (*b*) streamwise Reynolds stress profiles corrected using the proposed correction, using the measured value of $\overline{u^2}^+_m$ at $z^+ = 15$. Data from Hutchins *et al.* (2009).

4. Validation of the proposed correction

Here we test the correction method using streamwise Reynolds stress data acquired in boundary layers and fully developed pipe flows. The experiments were performed at matched Reynolds number, but with varying sized probes so that the spatial resolution effects could be evaluated. Figures 7 and 8 show the results for boundary layer flows at $Re_\tau = 7300$ and 13 600, respectively. The proposed correction collapses the data extraordinarily well, even with values of l^+ is as high as 153.

Figure 9 shows the results for pipe flow at $Re_\tau = 3000$ (here $Re_\tau = Ru_\tau/\nu$, where R is the pipe radius). The correction works as well here as it did for the boundary layer data.

In order to validate the correction method when no measurements at $z^+ = 15$ are available, (3.9) was used to evaluate M for the boundary layer data at $Re_\tau = 7300$. The corrected profiles are shown in figure 10, and the results are virtually identical to

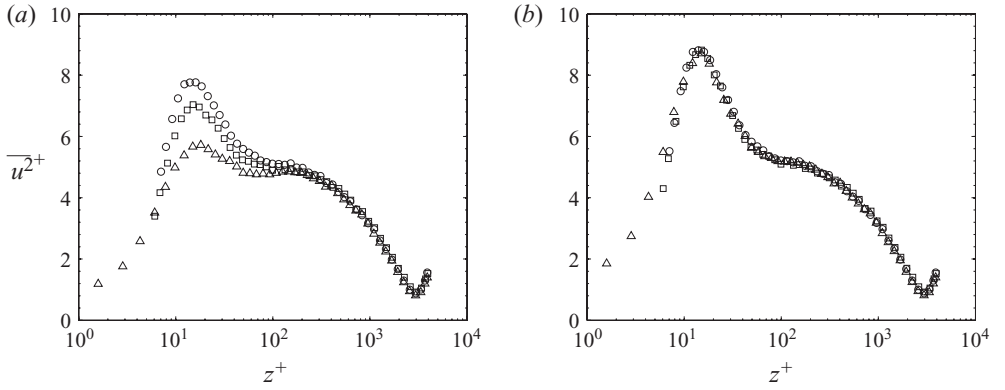

FIGURE 9. Streamwise Reynolds stress profiles measured in a fully developed turbulent pipe flow with various wire lengths at $Re_\tau = 3000$, where ○ $l^+ = 22$, □ $l^+ = 35$ and △ $l^+ = 62$: (*a*) uncorrected data, (*b*) streamwise Reynolds stress profiles corrected using the proposed correction, using the measured value of $\overline{u^2}^+_m$ at $z^+ = 15$. Data from Ng *et al.* (2011).

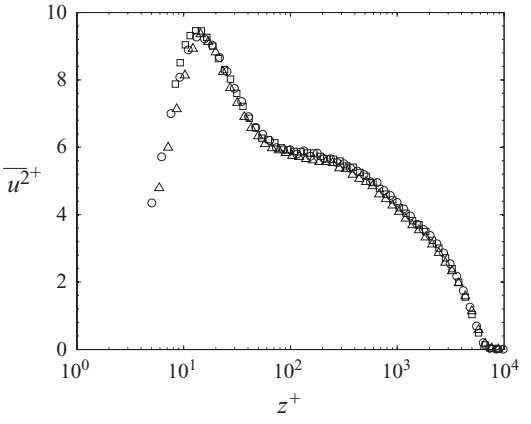

FIGURE 10. Streamwise Reynolds stress profiles measured in a fully developed turbulent boundary layer at $Re_\tau = 7300$ with various wire lengths, where ○ $l^+ = 22$, □ $l^+ = 79$ and △ $l^+ = 153$, corrected using M evaluated with (3.9). Data from Hutchins *et al.* (2009).

those shown in figure 7 where the measured value at $z^+ = 15$ was used, giving further confidence to the correction scheme proposed here.

5. Conclusions

The unresolved contribution to the streamwise Reynolds stress due to finite sensor size has been investigated for wall-bounded flows. The attached eddy hypothesis was used to predict that the attenuation would scale with l/z for $z^+ > 15$. This scaling differs from most other correction methods which use the viscous length scale instead. A functional form for the 'missing' streamwise Reynolds stress was then proposed that can be used to correct data acquired using inadequate probe size. The new formulation was found to work very well for boundary layer data as well as pipe flow data at three different Reynolds numbers.

The authors wish to acknowledge the support of the Australian Research Council, AOARD under Grant AOARD-09-4023 (Program Manager R. Ponnappan), AFOSR under Grant FA9550-09-1-0569 (Program Manager J. Schmisseur) and ONR under Grant N00014-09-1-0263 (Program Manager R. Joslin).

REFERENCES

Adrian, R. J. 2007 Hairpin vortex organization in wall turbulence. *Phys. Fluids* **19**, 041301.

Bailey, S. C. C., Kunkel, G. J., Hultmark, M., Vallikivi, M., Hill, J. P., Meyer, K. A., Tsay, C., Arnold, C. B. & Smits, A. J. 2010 Turbulence measurements using a nanoscale thermal anemometry probe. *J. Fluid Mech.* **663**, 160–179.

Cameron, J. D., Morris, S. C., Bailey, S. C. C. & Smits, A. J. 2010 Effects of hot-wire length on the measurement of turbulent spectra in anisotropic flows. *Meas. Sci. Technol.* **21**, 105407.

Carlier, J. & Stanislas, M. 2005 Experimental study of eddy structures in a turbulent boundary layer using particle image velocimetry. *J. Fluid Mech.* **535**, 143–188.

Chin, C. C., Hutchins, N., Ooi, A. S. & Marusic, I. 2009 Use of direct numerical simulation (DNS) data to investigate spatial resolution issues in measurements of wall-bounded turbulence. *Meas. Sci. Technol.* **20**, 115401.

DeGraaff, D. B. & Eaton, J. K. 2000 Reynolds-number scaling of the flat-plate turbulent boundary layer. *J. Fluid Mech.* **422**, 319–346.

Etter, R. J., Cutbirth, J., Ceccio, S., Dowling, D. & Perlin, M. 2005 High Reynolds number experimentation in the U.S. Navy's William B. Morgan large cavitation channel. *Meas. Sci. Technol.* **16**, 1701–1709.

Fernholz, H. H., Krause, E., Nockemann, M. & Schober, M. 1995 Comparative measurements in the canonical boundary layer at $Re_\theta \leqslant 6 \times 10^4$ on the wall of the DNW. *Phys. Fluids* **7**, 1275–1281.

Hultmark, M. N., Bailey, S. C. C. & Smits, A. J. 2010 Scaling of near-wall turbulence in pipe flow. *J. Fluid Mech.* **649**, 103–113.

Hutchins, N., Nickels, T. B., Marusic, I. & Chong, M. S. 2009 Hot-wire spatial resolution issues in wall-bounded turbulence. *J. Fluid Mech.* **635**, 103–136.

Jiménez, J. M., Hultmark, M. & Smits, A. J. 2010 The intermediate wake of a body of revolution at high Reynolds number. *J. Fluid Mech.* **659**, 516–539.

Kline, S. J., Reynolds, W. C., Schraub, F. A. & Rundstadler, P. W. 1967 The structure of turbulent boundary layers. *J. Fluid Mech.* **30**, 741–773.

Lagerlof, R. O. E. 1974 Interpolation with rounded ramp functions. *Commun. ACM* **17** (8), 476–497.

Ligrani, P. M. & Bradshaw, P. 1987 Subminiature hot-wire sensors: development and use. *J. Phys. E: Sci. Instrum.* **20**, 323–332.

Marusic, I. & Kunkel, G. J. 2003 Streamwise turbulence intensity formulation for flat-plate boundary layers. *Phys. Fluids* **15**, 2461–2464.

Marusic, I., McKeon, B. J., Monkewitz, P. A., Nagib, H. M., Smits, A. J. & Sreenivasan, K. R. 2010 Wall-bounded turbulent flows: recent advances and key issues. *Phys. Fluids* **22**, 065103.

Metzger, M. M. & Klewicki, J. C. 2001 A comparative study of near-wall turbulence in high and low Reynolds number boundary layers. *Phys. Fluids* **13** (3), 692–701.

Mochizuki, S. & Nieuwstadt, F. T. M. 1996 Reynolds-number-dependence of the maximum in the streamwise velocity fluctuations in wall turbulence. *Exp. Fluids* **21**, 218–226.

Monkewitz, P. A., Duncan, R. D. & Nagib, H. M. 2010 Correcting hot-wire measurements of stream-wise turbulence intensity in boundary layers. *Phys. Fluids* **22**, 091701.

Morrison, J. F., McKeon, B. J., Jiang, W. & Smits, A. J. 2004 Scaling of the streamwise velocity component in turbulent pipe flow. *J. Fluid Mech.* **508**, 99–131.

Nagib, H. M., Chauhan, K. A. & Monkewitz, P. A. 2007 Approach to an asymptotic state for zero pressure gradient turbulent boundary layers. *Phil. Trans. R. Soc. Lond.* A **365**, 755.

Ng, H., Monty, J., Hutchins, N., Chong, M. & Marusic, I. 2011 Comparison of turbulent channel and pipe flows with varying Reynolds number. *J. Fluid Mech.* (submitted).

Nickels, T. B., Marusic, I., Hafez, S. M., Hutchins, N. & Chong, M. S. 2007 Some predictions of the attached eddy model for a high Reynolds number boundary layer. *Phil. Trans. R. Soc. Lond.* A **365**, 807–822.

Österlund, J. M., Johansson, A. V., Nagib, H. M. & Hites, M. H. 2000 A note on the overlap region in turbulent boundary layers. *Phys. Fluids* **12** (1), 1–4.

Perry, A. E. & Chong, M. S. 1982 On the mechanism of wall turbulence. *J. Fluid Mech.* **119**, 173–217.

Saddoughi, S. G. & Veeravalli, S. V. 1994 Local isotropy in turbulent boundary layers at high Reynolds number. *J. Fluid Mech.* **268**, 333–372.

Stanislas, M., Perret, L. & Foucaut, J.-M. 2008 Vortical structures in the turbulent boundary layer: a possible route to a universal representation. *J. Fluid Mech.* **602**, 327–382.

Townsend, A. A. 1976 *The Structure of Turbulent Shear Flow*. Cambridge University Press.

Winkel, E., Oweis, G., Cutbirth, J., Ceccio, S., Perlin, M. & Dowling, D. 2010 The mean velocity profile of a smooth flat-plate turbulent boundary layer at high Reynolds number. *J. Fluid Mech.* **665**, 357–381.

Wyngaard, J. C. 1968 Measurements of small scale turbulence structure with hot-wires. *J. Sci. Instrum.* **1**, 1105–1108.

Yakhot, V., Bailey, S. C. C. & Smits, A. J. 2010 Scaling of global properties of turbulence and skin friction in pipe and channel flows. *J. Fluid Mech.* **652**, 65–73.

Zagarola, M. V. & Smits, A. J. 1998 Mean-flow scaling of turbulent pipe flow. *J. Fluid Mech.* **373**, 33–79.